POLARIZATION MEASURES AND NATURE OF DARK ENERGY

L.P.L. Colombo, R. Mainini & S.A. Bonometto

Physics Dep. G. Occhialini, Università degli Studi di Milano–Bicocca, Piazza della Scienza 3, I20126 Milano (Italy) & I.N.F.N., Via Celoria 16, I20133 Milano (Italy)

Abstract.   Polarization measures, on wide angular scales, together with anisotropy data, can fix DE parameters. Here we discuss the sensitivity needed to provide significant limits. Our analysis puts in evidence that a class of models predicts low correlation or anticorrelation between polarization and anisotropy at low l. This class includes open models and models with DE due to a Ratra–Peebles (RP) potential. Results on this point, given in a previous paper of ours, are updated and partially corrected. We outline that, with the sensitivity of experiments like SPOrt or WMAP, high values of Λ (energy scale in the RP potential) can be excluded. With the sensitivity expected for PLANCK, the selection will extend to much lower Λ's.

1   Introduction

The nature of Dark Energy (DE) is one of the main puzzles of cosmology. DE was first required by SNIa data [1], but a *flat* Universe with $\Omega_m \simeq 0.3$ and $\Omega_b h^2 \simeq 0.02$ is also favored by CBR and LSS observations [2,3] ($\Omega_{m,b}$: matter, baryon density parameters; h: Hubble parameter in units of 100 km/s/Mpc; CBR: cosmic background radiation; LSS: large scale structure).

DE could be a false vacuum; then, its pressure and energy density (p_{DE} and ρ_{DE}) have ratio $w = -1$. This however requires a severe fine tuning at the end of the EW transition. Otherwise, DE can be a scalar field ϕ self–interacting through a potential $V(\phi)$ (dynamical DE [4,5,6]). Then

$$\rho_{DE} = \dot{\phi}^2/2a^2 + V(\phi) \ , \quad p_{DE} = \dot{\phi}^2/2a^2 - V(\phi) \quad (1.1)$$

(derivatives are in respect to the conformal time t). As soon as $\rho_k = \dot{\phi}^2/2a^2 < V$, it is $w < 0$ For $\rho_k/V \simeq 1/2$, it is $w \simeq -1/3$ and dynamical DE approaches an open CDM behavior. Smaller ρ_k/V ratios approach $w = -1$ and a ΛCDM behavior. To work out $w(a)$, the Friedman equations, together with the equation of ϕ, are to be integrated; the solutions depend on the shape of V, which, in principle, is largely arbitrary.

Among potentials admitting a *tracker* solution, the RP [5] and SUGRA [6] expressions

$$V(\phi) = \Lambda^{4+\alpha}/\phi^\alpha \ , \qquad V(\phi) = (\Lambda^{4+\alpha}/\phi^\alpha)\exp(4\pi\phi^2/m_p^2) \ , \quad (1.2)$$

are particularly relevant, as they originate within the frame of Supersymmetric (SUSY) theories. Here, Λ is an energy scale, set in the interval 1–10^{12} GeV; m_p is the Planck mass. Once Λ and Ω_{DE} are fixed, the exponent α is set. RP and SUGRA potentials yield fast and slowly varying w, respectively.

Dynamical DE and ΛCDM often predict similar observational outputs. This is welcome, as ΛCDM is a good fit to data. However, here we show that measures of anisotropy and polarization of CBR, at large angular scales, constrain V and distinguish dynamical DE from ΛCDM. Accordingly, experiments in progress already exclude some parameter range for RP models and higher sensitivities can discriminate even better. In a previous paper [7], similar results were provided; that paper, however, contained a numerical mistake. Here we correct some of its quantitative results.

Our procedure includes a likelihood analysis, assuming polarization data provided by the Sky Polarization Observatory [8], both with the expected experimental noise level and a higher sensitivity. Results, however, can be straightforwardly extended to other observational contexts.

2   CMB angular spectra from the Boltzmann equations; theory

The angular CBR spectra $C_l^{T,E,TE}$ (only E–mode is considered through this paper) can be worked out from the linear fluctuation evolution, obtained by solving the Boltzmann equation for the photon

distribution. The treatment is discussed in a number of papers [9], giving also the equations for the other components of a model. In this section we show that these equations, in several cases, yield a low or negative C_l^{TE} for low l. All definitions used are the same as in CMBFAST [10].

This effect arises because of the simultaneous action of the ISW effect and of the opacity $\tau = \int_t^{t_o} n_e(t')\sigma_T a(t')\,dt'$. (Notice that $-\dot{\tau} = a\,n_e\sigma_T$); n_e and σ_T are the free electron density and the Thomson cross–section. ISW effect arises when we pass either from matter to curvature dominance (open models) or from matter to vacuum dominance (ΛCDM models). However, only in the former case and in the presence of opacity, anticorrelation arises. Some RP models induce anticorrelation because their features more closely approach open CDM, rather than ΛCDM.

Let us then indicate by $F_l(k,t)$ and $G_l(k,t)$ the Boltzmann components for anisotropy and polarization (k is the wave–number). The equations for the G_l components in flat models read:

$$\dot{G}_l = -\dot{\tau}\left[-G_l + \frac{\Pi}{2}(\delta_{l0} + \frac{\delta_{l2}}{5})\right] + \frac{k}{2l+1}[l\,G_{l-1} - (l+1)G_{l+1}] \tag{2.1f}$$

(δ_{ln} is the Kronecker symbol). Here
$$\Pi = G_o + G_2 + F_2, \tag{2.2}$$

is the only vehicle from anisotropy to polarization. In open models, eq. (2.1f) becomes:

$$\dot{G}_l = -\dot{\tau}\left[-G_l + \frac{\Pi}{2}(\delta_{l0} + \frac{\delta_{l2}}{5})\right] + \frac{\beta}{2l+1}[lb_l\,G_{l-1} - (l+1)b_{l+1}G_{l+1}] \;; \tag{2.1o}$$

here $\beta^2 = k^2 + K$ and $b_l^2 = 1 - Kl^2/\beta^2$, with $K = -(1-\Omega_m)H_0^2$, H_0 is today's Hubble parameter.

Initially all G_l terms are zero; to switch them on, the quadrupole $F_2(k,t)$ must be great when n_e is not so low. For wavelengths $2\pi/k$ entering the horizon well after recombination, $F_2(k,t)$ switch on when n_e has almost vanished, unless reionization occurs. Notice that the horizon size at recombination corresponds to $l \ll 200$. Without reionization, below such l, we expect low G_l's.

Let F_l^o (G_l^o) be the present value of harmonics. In spatially flat models, the angular spectra read

$$C_l^T = \frac{\pi}{4}\int d^3k\,P_o(k)\,|F_l^o(k)|^2 \;,\; C_l^P = \frac{\pi}{4}\int d^3k\,P_o(k)\,|G_l^o(k)|^2 \;,\; C_l^{TE} = \frac{\pi}{4}\int d^3k\,P_o(k)\,F_l^o(k)G_l^o(k), \tag{2.3f}$$

$P_o(k)$ being the primeval fluctuation spectrum. In open model, instead, they read

$$C_l^T = \frac{\pi}{4}\int d^3\beta\,P_o(q)\,|F_l^o(\beta)|^2 \;,\; C_l^P = \frac{\pi}{4}\int d^3\beta\,P_o(q)\,|G_l^o(\beta)|^2 \;,\; C_l^{TE} = \frac{\pi}{4}\int d^3\beta\,P_o(q)\,F_l^o(\beta)G_l^o(\beta) \;; \tag{2.3o}$$

here $q = (\beta^2 - 4K)^2/\beta(\beta^2 - K)$. Clearly, for $\Omega_m = 1$, both β and q return k.

Comparing eqs. (2.1) and (2.3) shows suitable shifts in the k–space. In particular, the b_l coefficients cause a shift of C_l peaks, while the passage from k to β and q, in eq. (2.3o), displace the power through the harmonics F_l at small l, i.e. on scales comparable with the curvature scale. Apart of these shifts, the gravitational field fluctuations ($\dot{h}$ and η) obey similar but different equations:

Open models :
$$2\bar{k}^2\dot{\eta} = 8\pi Ga^2\left[\sum_c(\rho_c + p_c)\theta_c - \dot{h}\rho_{o,cr}(1 - \Omega_m)/a^2\right]. \tag{2.4o}$$

Flat models :
$$2k^2\dot{\eta} = 8\pi Ga^2\left[\sum_c(\rho_c + p_c)\theta_c + (\rho_{DE} + p_{DE})\theta_{DE}\right]. \tag{2.4f}$$

Here $\sum_c$ sums over all (relativistic or non–relativistic) matter components apart of DE; $\rho_{o,cr}$ is today's critical density. The wave–numbers $\bar{k}^2$ and k^2 are just shifted by $3K$.

Notice that, in a ΛCDM model, no DE fluctuations exist while $\rho_{DE} = -p_{DE}$, so that the second term at the r.h.s. of eq. (2.4f) vanishes. In models with dynamical DE, instead, $\theta_{DE} \neq 0$ and $\rho_{DE} \neq -p_{DE}$. Accordingly, the second term in square brackets in eq. (2.4f) may read $\theta_{DE}\rho_{o,cr}(1 - \Omega_m)(1 + w)(\rho_{DE}/\rho_{o,DE})$ (the last parenthesis tells us how DE energy scales with a). This term is analogous to the second term in square bracket in eq. (2.4o) and would coincide with it if $w = -1/3$ and, namely, if $\theta = -\dot{h}/2$. If this is true, apart of a different power distribution along the l axis and
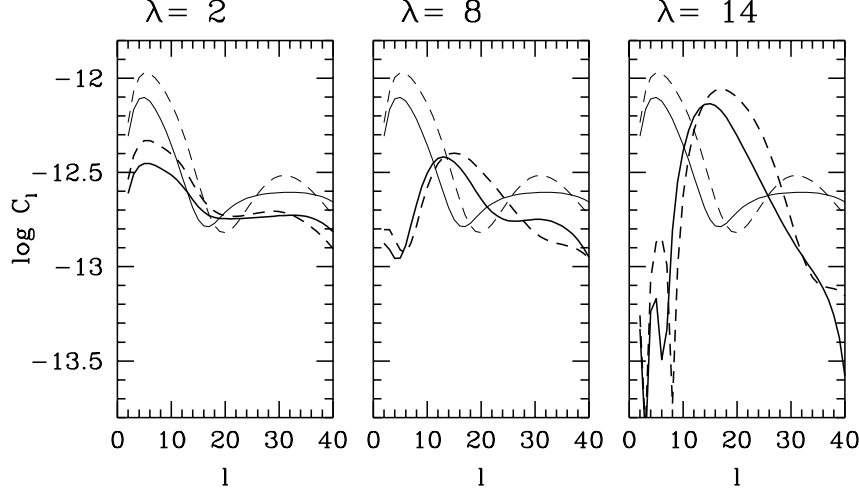
Figure 1: TE correlation spectra $[C_l = l(l+1)|C_l^{TE}|/4\pi]$ for ΛCDM (the same in the three plots) and RP. Solid (dashed) lines refer to $\tau = 0.14$ (0.20). In the third plot, low–l peaks are negative.

geometric effects at greater l, there can be similarities in the behavior of open and dynamical DE models. The relation between $\dot{h}/2$ and θ_{DE} can then be studied through the equation

$$\theta_{DE} + \frac{\dot{h}}{2} = -\frac{1}{1+w} [\dot{\delta}_{DE} + 3\frac{\dot{a}}{a}(c_s^2 - w)\delta_{DE}], \qquad (2.5)$$

whose validity indicates that DE behaves as a fluid. An order of magnitude estimate, however, tells us soon that $\theta_{DE} \sim k^2 t\, \delta_{DE}$; then, the ratio between θ_{DE} and the r.h.s. is $\sim (t/L)^2$, where L is the scale related to k. Before horizon crossing ($t \ll L$), the θ_{DE} term is negligible, in comparison with the r.h.s.. Hence, $\dot{h}/2$ equates the r.h.s. and, therefore, the ratio $-\dot{h}/2\theta_{DE}$ exceeds unity. At horizon crossing such ratio must approach unity and keep such as t grows greater than L. The main differences between open and dynamical DE models, in the r.h.s. of eqs. (2.4) are therefore relegated to times before horizon crossing. Afterward, the residual difference is due to a factor $1 + w$.

The changes in $\dot{\eta}$ directly act on F_2. The equation fulfilled by this spectral component reads:

$$\dot{F}_2(k,t) = -\dot{\tau}\left[-F_2(k,t) + \frac{\Pi(k,t)}{10}\right] + \frac{k}{5}[2\,F_1(k,t) - 3F_3(k,t)] + \frac{8}{5}\left(\dot{\eta}(k,t) + \frac{\dot{h}(k,t)}{6}\right) \qquad (2.6f)$$

in flat models, while in open models we have:

$$\dot{F}_2(\beta,t) = -\dot{\tau}\left[-F_2(\beta,t) + \frac{\Pi(\beta,t)}{10}\right] + \frac{\beta}{5}[2b_2\,F_1(\beta,t) - 3b_3 F_3(\beta,t)] + \frac{8}{5}\frac{\beta}{k}b_2\left(\dot{\eta}(\beta,t) + \frac{\dot{h}(\beta,t)}{6}\right). \qquad (2.6o)$$

Accordingly, when open models show negative TE correlations at low l, we expect something similar in flat RP models. On the contrary, models like SUGRA, with a cosmic acceleration closer to ΛCDM models, are not expected to give negative TE correlation.

Let us then discuss how the likelihood distribution can be obtained from model spectra, taking into account that the number of pixels for anisotropy and polarization (N_T and N_P) in our (artificial) data are different. Let T_j be the anisotropy data measured in N_T pixels and Q_j and U_j be the Stokes parameters in N_P pixels. In general, let be $\mathbf{x} \equiv (T_1, ..., T_{N_T}, Q_1, ..., Q_{N_P}, U_1, ..., U_{N_P})$. $\mathbf{x}$ is a vector of $N_s = N_T + 2N_P$ components, defining an observed state of anisotropy and polarization. Once a model is assigned, the C_l are uniquely determined. Passing to a data vector $\mathbf{x}$, instead, amounts to performing a model realization. _Vice–versa_, once the N_s component data vector $\mathbf{d}$ is given, the model is not uniquely fixed.
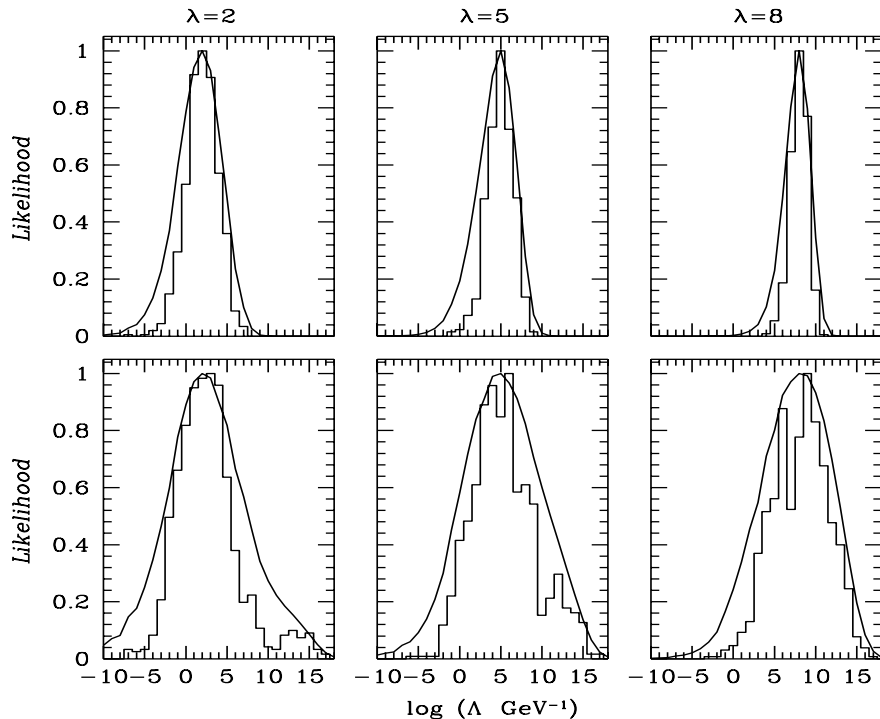
Figure 2: Histograms give the distribution of peak likelihood. Continuous curves give the likelihood distribution averaged over realizations (arbitrary but equal normalization). Pixel noise is $0.2\,\mu\text{K}$ in the upper panels and $2\,\mu\text{K}$ in the lower panels; all plots refer to $\tau = 0.14$.

Then, the likelihood of a model, whose angular spectra are C_l, when the data $\mathbf{d}$ are observed, reads

$$L(\mathbf{d}|C_l^A) \propto [\det \mathbf{M}]^{-\frac{1}{2}} \exp\left[-\frac{1}{2}\mathbf{d^T M^{-1} d}\right] . \tag{2.7}$$

The main ingredient of L is the correlation matrix $\mathbf{M_{ij}} = \langle \mathbf{x}_i^T \mathbf{x}_j \rangle = \mathbf{S}_{ij} + \mathbf{N}_{ij}$; here $\mathbf{S}_{ij}$ is the signal term and $\mathbf{N}_{ij}$ is due to the noise. The components $\mathbf{M_{ij}}$ yield the expected correlation between the ith and jth elements of data vectors $\mathbf{x}$ corresponding to particular choices of C_l [10]. The construction of the noise term is simpler, as we expect no noise correlation, and the matrix $\mathbf{N}_{ij} = \delta_{ij}\,\sigma_{T,pix}{}^2$ (for $i = 1, ..., N_T$) and $\mathbf{N}_{ij} = \delta_{ij}\,\sigma_{P,pix}{}^2$ (for $i = N_T + 1, ..., N_s$) is diagonal.

3 Angular spectra and likelihood: results.

In Fig. 1 we show the spectra C_l^{TE} for ΛCDM and RP models, if $\tau = 0.14$ and $\tau = 0.20$ (WMAP[11] suggests that $\tau = 0.17 \pm 0.04$). The value of $\lambda = \log_{10}(\Lambda/\text{GeV})$ is given in top of the frames. Low–l anticorrelation is found only for $\lambda > \sim 10$ and is shown in the third plot. The differences between ΛCDM and RP increase for growing λ, but are already significant even for $\lambda = 2$.

At low l, cosmic variance must be taken into account, aside of instrumental variance. We then perform a large number (1000) of realizations of RP sky models for $\lambda =$2, 5 and 8, for $\tau = 0.14$ and 0.20. In Fig. 2 (3) we report report results for $\tau = 0.14$ (0.20). The values of λ are shown in top of each plot. Lower and upper plots correspond to $\sigma = 2$ and $0.2\,\mu\text{K}$, respectively. The former value approaches WMAP and SPOrt expectations; the latter value might be approached by the PLANCK [12] experiment.

4 Conclusions

These figures show that, as expected, RP models are more easily distinguishable from ΛCDM for lower σ and higher λ. We can assume that a RP model gives a signal different from ΛCDM when $\lambda > 0$ is detected. However, even in the less favorable case considered, when $\sigma = 2\,\mu\text{K}$, $\tau = 0.14$ and $\lambda = 2$, the peak likelihood is at $\lambda > 0$ in $\sim 72\,\%$ of cases. For $\lambda = 5$, this fraction reaches $\sim 91\,\%$. Likelihood distributions, averaged both over cosmic and instrimental variances, tell us that RP models begin to
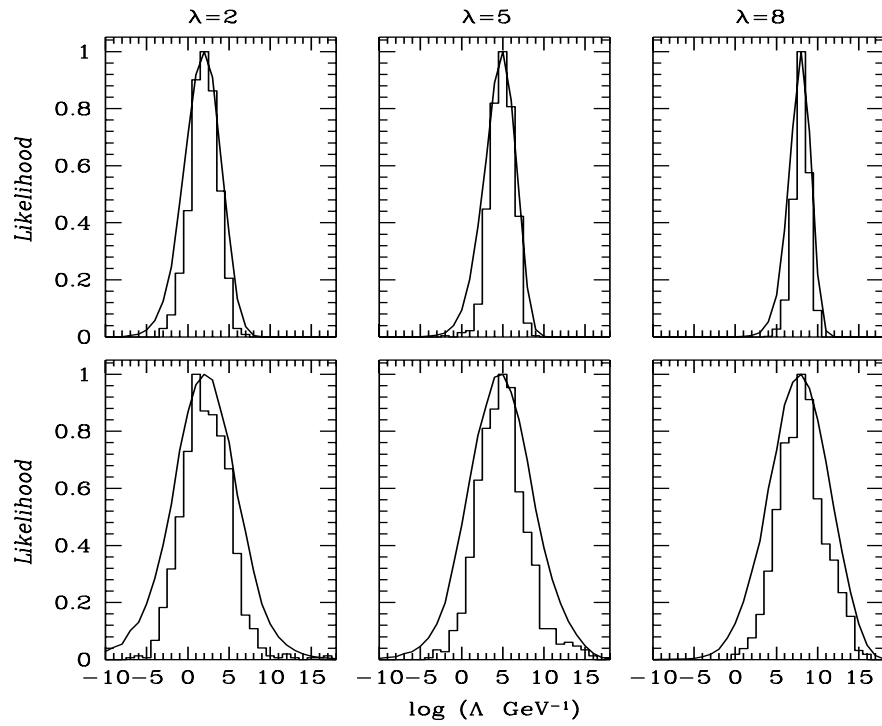
Figure 3: The same as Fig. 2, but for an optical depth of $\tau = 0.20$.

be distinguishable from ΛCDM, at 1–σ level, for $\lambda \sim 5$ and $\tau = 0.20$, if $\sigma = 2\,\mu$K. For $\sigma = .2\,\mu$K, instead, this is already true for $\lambda = 2$. See the figures for further details.

A general conclusion that can be drawn from this analysis is that cosmic variance is far from being a serious limit to model parameter detection from large angle spectral analysis, at the present sensitivity levels. Even for a sensitivity improved by a factor 10, hystograms are still contained inside the curve, showing that there is a relevant space for further improvements.

References

[1] Perlmutter S et al., 1998, Nature 391, 51; Riess A G et al., 1998, AJ 116, 1009

[2] Tegmark M et al., 2001,Phys Rev D, 63, 43007; Netterfield C B et al., 2002, ApJ, 571, 604

[3] Percival W J et al., 2002, MNRAS, in press; Efstathiou G et al., 2002, MNRAS, 330, L29; Schuecker P et al., 2003, A & A, in press; Pogosian D et al., 2003

[4] Wetterich C, 1988, Nucl.Phys.B, 302, 668; Wetterich C, 1995, A & A, 301, 321; Ferreira & Joyce 1998; Perrotta F & Baccigalupi C, 1999, Phys. Rev. D, 59, 123508; Steinhardt P J et al., 1999, Phys. Rev. D, 59, 12350; Zlatev I et al., 1999, Phys Rev Lett, 82, 896; Albrecht A & Skordis C, 2000, Phys. Rev. Lett., 84, 2076; Amendola L, 2000, Phys. Rev. D, 62, 043511

[5] Ratra B & Peebles P J E, 1988, Phys Rev D, 37, 3406

[6] Brax P et al. 2000, Phys.Rev. D, 62, 103505; Brax P & Martin J, 1999, Phys.Lett., B468, 40; Brax P & Martin J, 2000, Phys. Rev. D, 61, 103502

[7] Mainini et al., 2003, New Ast, in press

[8] http://sport.bo.iasf.cnr.it

[9] see, e.g., Ma C P & Bertshinger E, 1995, ApJ, 455, 7

[10] http://physics.nyu.edu/matiasz/CMBFAST/cmbfast.html; Zaldarriaga M, 1998, ApJ, 503, 1

[11] http://lambda.gsfc.nasa.gov/product/map/m_overview.html

[12] http://astro.estec.esa.nl/Planck/